RSC Advances

This article can be cited before page numbers have been issued, to do this please use: Y. Wang, R. Priambodo, H. Zhang and Y. Huang, *RSC Adv.*, 2015, DOI: 10.1039/C5RA04238K.

ROYAL SOCIETY OF CHEMISTRY

www.rsc.org/advances

View Article Online
DOI: 10.1039/C5RA04238K

RSC Advances

RSC Advances

ARTICLE

Degradation of Azo Dye Orange G in fluidized bed reactor using iron oxide as a heterogeneous photo-Fenton catalyst

Cite this: DOI:

Received,
Accepted

DOI:

www.rsc.org/

Y. Wang[a,b,c], R. Priambodo[c], H. Zhang[a,†] and Y.H. Huang[c,d,†]

Abstract: The heterogeneous Fenton process was employed to degrade Orange G (OG) using waste iron oxide as the catalyst in a three-phase fluidized bed reactor (3P-FBR). The morphology and the FTIR spectra of used BT4 were compared with fresh catalyst to illustrate the catalyst stability. The catalyst reusability was evaluated by measuring colour removal in four successive cycles. The effect of major parameters, including pH, H_2O_2 concentration and catalyst addition on the decolorization of OG was investigated. The satisfactory decolorization efficiency (> 92%) could be obtained under the conditions tested, and 78.9% of TOC removal was achieved at 50 mg L^{-1} initial OG concentration, 25 mg L^{-1} H_2O_2 concentration, pH = 3 and 6 g L^{-1} BT4 addition. The decolorization of OG was mainly attributed to the homogeneous photo-Fenton reaction, while the heterogeneous catalytic process played an important role in TOC removal. The main intermediates were identified by GC/MS technique and the degradation pathway of OG was proposed.

Keywords: waste iron oxide; degradation pathway; heterogeneous Fenton-like catalyst; orange G

1. Introduction

In recent years, the treatment of textile and dyeing wastewater coming from textile industries and other related industries has received the increasing attention because of the high yield, the low biodegradability and the high toxicity of these wastewaters.[1-5] As one of azo dyes used widely, Orange G (OG) is characterized by one azo group (–N=N–) bound to aromatic rings and auxochromes (–OH, –SO_3, etc.).[6-8] Moreover, the azo group is responsible for producing the colour while auxochromes enhance the affinity of the dye towards the fibres and water.[9,10] The widespread utilization of OG in different domains has caused a serious environmental problem due to its obvious and latent danger for humans and ecosystem.[8,10] Therefore, various treatment processes have been employed for the OG removal from aqueous solution, such as biological treatment [11] and adsorption[10]. Biological process is the most commonly used method for the wastewater treatment, but it has been proved to be inefficient for dye removal.[11,12] Adsorption is also extensively applied for the dye wastewater treatment, but it only transfers the contaminants from one medium to another and further disposal is needed.[13-15] As a result, the development of powerful and effective oxidation processes is required urgently to remove OG and its by-products from wastewater.[16]

Over the past decades, advanced oxidation processes (AOPs) have been proved to be effective for the removal of toxic and/or bio-refractory organic pollutants.[5-7,17] Among AOPs, Fenton process offers the cost-effective source of hydroxyl radicals and is easily operated and maintained.[18-20] However, the application of homogeneous Fenton process is restricted by the difficulty and expensive cost for the disposal of the large amount of iron sludge.[21,22] To overcome these drawbacks, heterogeneous Fenton process using inexpensive, efficient, stable, and easily prepared and separated catalysts has been developed, as a potential alternative for the treatment of dye wastewater containing OG.[9,12,22-24] Among these catalysts, iron oxides and iron supported catalysts exhibit high activity to accelerate the decomposition of H_2O_2 and are considered to be the most promising catalysts.[4,22-31] In this study, the feasibility of waste iron oxide (labeled as BT4), as a cheap photo-Fenton catalyst, was investigated for the OG degradation. BT4 is a by-product resulting from the non-seeded fluidized-bed Fenton reaction for the treatment of the bio-effluent tannery wastewater from a dyeing plant in Taiwan.[32-34]

Due to the simplicity of its design and construction, low operating cost, high flexibility for liquid and solid phase residence times and temperature control, heterogeneous Fenton process combined with fluidized bed reactor (FBR) has been widely used for the treatment of wastewater.[35,36] To further improve the contact between different phases, mass transfer capacity and the mixing properties with low power requirements, a novel three-phase fluidized bed reactor (3P-FBR) was proposed in our previous studies.[34, 37] In this work, OG, as a model azo dye, was treated by the heterogeneous photo-Fenton process in 3P-FBR. The effect of operating conditions on the removal of OG was investigated to explore the mechanism of this process. The intermediate products were identified and the degradation pathway of OG was proposed.

2. Experiment

2.1 Materials

Orange G (OG, $C_{16}H_{10}N_2Na_2O_7S_2$) was purchased from Sigma and had a molecular weight of 452.38. H_2O_2 (50 wt%, Union Chemical Works, Taiwan) was of analytical reagent grade and used without further purification. Other chemicals used herein, including sulfuric acid and sodium hydroxide, were of analytical grade and were used to adjust pH. Deionized and doubly distilled water were used throughout this investigation.

View Article Online
DOI: 10.1039/C5RA04258K
RSC Advances

The iron oxide (BT4), a by-product of the FBR-Fenton reaction for the treatment of the bio-effluent from tannery wastewater, was withdrawn from FBR after 4 months. It comprises mainly goethite (α-FeOOH phase) with lower crystallinity, which has been verified in our previous studies.[32-34] The physical properties of the BT4 were as follows: 1.54 g cm^{-3} of the bulk density, 2.50 g cm^{-3} of absolute density, and 150 m^2 g^{-1} of the specific surface area.[34]

2.2 Experimental procedures

All experiments were carried out in a 3P-FBR containing 1.5 L solution at room temperature (25 °C) under the UV irradiation (Fig. 1). The reactor consists of coaxial cylinder with inner and outer diameters of 35 and 70 mm and the heights of these two cylinders were 300 and 450 mm, respectively. The porous sintered plate was located at a distance of 35 mm from the bottom of the reactor to ensure a uniform distribution of air. The irradiation source was a 15W UV lamp (UVP BL-15 365 nm) fixed inside a cylindrical pyrex tube (allowing wavelengths λ > 320 nm to pass) and the UV light was turned on for 10 min to stabilize the irradiation before starting the experiment. Air bubbles were injected continuously from the bottom of fluidized bed reactor to circulate the BT4 particles throughout the reactor. Solution pH was adjusted by H_2SO_4 or NaOH and measured with a pH meter (Action, A211). The predetermined quantity of BT4 and H_2O_2 was dripped into the reactor. The reaction time was recorded immediately after H_2O_2 was applied. Samples were taken from the reactor periodically using a pipette, and NaOH was added immediately to quench the reaction after filtration by a 0.22 μm syringe filter made of poly-(vinylidene fluoride).

Fig. 1.

2.3 Analysis

The absorbance of OG was measured at λ_{max} = 480 nm using an Agilent 8453 UV-Visible spectrophotometer. The intermediate products were identified by GC/MS with a HP-5MS capillary column (30 m × 0.25 mm × 0.25 μm) which was employed for molecule separation (GC HP series 6890). A 200 mL dye solution was extracted with 25 mL of dichloromethane for 4 times. Then the organic phases were concentrated to about 2 mL by a rotary evaporator at 40 °C before GC/MS analyses. A temperature programmed mode was used. The initial temperature of 40 °C was held for 10 min, and ramped at 12 °C min^{-1} to 100 °C, then to 200 °C with a 5 °C min^{-1} rate, and finally ramped at 20 °C min^{-1} to 270 °C, followed by an isothermal time of 5 min.

The total iron leached from BT4 was determined by atomic absorption spectrophotometry (Sens AA). TOC was measured using a TOC analyzer (Sievers Innovox Laboratory TOC Analyzer). The carboxylate ion was analyzed by ion chromatography (IC, Dionex DX-120). Morphology of BT4 was determined using a Hitachi S-400 scanning electron microscope (SEM). The infrared spectra of BT4 were recorded on KBr pellets by a Fourier transform infrared spectrometer (FTIR, Nicolet Avatar 330). To avoid moisture, KBr pellets were prepared by pressing mixtures of dry powered sample and spectrometry-grade KBr under vacuum. 150 scans were collected for each sample in the range of 400–4000 cm^{-1} with a resolution of 2 cm^{-1}.

3. Results and discussion

3.1 Performance comparison between 3P-FBR and conventional FBR

The degradation of OG by heterogeneous photo-Fenton process was performed in 3P-FBR and conventional FBR (without internal draft tube), respectively. As shown in Fig. 2, the higher decolorization and TOC removal rates of OG were achieved in 3P-FBR than those in conventional FBR. In addition to the advantages of the conventional FBR such as the excellent contact between the reactants as well as the high mass and heat transfer rates, the 3P-FBR with an internal draft tube can obtain smooth and steady circulation of the catalyst particles in the bed.[3,38] This would improve the performance of the reactor. Therefore, the 3P-FBR was used in the following experiments.

Fig. 2.

3.2. Decolorization of OG by different treatment processes

The experiments were conducted in H_2O_2, BT4, UV, H_2O_2/BT4, UV/H_2O_2, UV/BT4 and UV/H_2O_2/BT4 system, respectively to illustrate the photo-catalytic potential of BT4. As shown in Fig. 3, the colour hardly decreased when UV alone was applied to OG solution. It is due to the fact that only a small amount of $^{\bullet}OH$ is formed in the presence of only UV irradiation.[34,39] The addition of H_2O_2 alone could not result in significant colour removal after 90 min treatment because of the limit oxidizing power of H_2O_2 (E^0 = 1.78 V).[21,34, 39] In control experiments, it was also confirmed that little colour removal was achieved when BT4 alone was added to solution, indicating that the effect of BT4 adsorption on OG removal was not obvious at pH 3. Although H_2O_2 could be decomposed by UV irradiation to generate $^{\bullet}OH$ when the UV wavelength was less than 300 nm,[40] little amount of $^{\bullet}OH$ was produced at UV wavelength > 300 nm (365 nm in this study). Therefore, the decolorization efficiency was also insignificant. Similarly, BT4 could not be photocatalyzed by 365 nm UV to produce $^{\bullet}OH$ and OG decolorization could be neglected in UV/BT4 system. However, BT4 could catalyze H_2O_2 to generate $^{\bullet}OH$, resulting in an 88.6% of decolorization efficiency after 90 min reaction through Eq. (1):

$$\equiv Fe^{2+} + H_2O_2 \rightarrow \equiv Fe^{3+} + {}^{\bullet}OH + OH^- \quad (1)$$

where the symbol ≡ represents the iron species bound to the surface of the catalyst.

Moreover, this process could be improved by UV [31,41-42] and the OG decolorization efficiency rose to 99.1% in the UV/H_2O_2/BT4 system. This will be discussed in the following section.

Fig. 3.

3.3. The degradation mechanism of OG in UV/H_2O_2/BT4 system

It has been reported that homogeneous catalytic mechanism was also involved in iron-based heterogeneous Fenton systems due to the leaching of iron from the catalyst.[31,43-46] Therefore, to ascertain the contribution of homogeneous photo-Fenton reaction induced by leached iron ion, the total iron concentration was monitored during the reaction. As can be seen in Fig. 4a, the dissolved iron increased firstly, reached a maximum value of 1.4 mg L^{-1}, and then decreased gradually. The $\equiv Fe^{3+}$ of BT4 surface could complex with carboxylate ion formed by the degradation OG. It resulted in the non-reductive dissolution of BT4 and accompanied by the increasing total iron concentration in the form of ferric carboxylate complexes.[47] When carboxylate was further degraded, the free Fe^{3+} would be released and then precipitated and/or crystallized onto the carrier (BT4) surface in 3P-FBR, leading to the decrease of dissolved iron concentration.[35,47]

To investigate the role of leached iron on the OG decolorization, homogeneous photo-Fenton experiment was carried out with 1.4 mg L^{-1} of soluble Fe^{2+}. As can be seen from Fig. 4b, 90.4% of decolorization efficiency was achieved after 90 min reaction. This phenomenon is consistent with our previous studies.[48] It illustrated that a satisfactory colour removal could be obtained via Fenton

RSC Advances View Article Online DOI: 10.1039/C5RA04238K ARTICLE

process even at a low iron concentration[48]. However, as low as 9.2% of mineralization efficiency was removed after 90 min reaction and TOC removal rose to only 20.2% even if the reaction time was extended to 180 min. This was much lower than 78.9% of TOC removal achieved in heterogeneous photo-Fenton ($UV/H_2O_2/BT4$) system. Based on the results, it can be concluded that the decolorization of OG was mainly attributed to the homogeneous photo-Fenton reaction, while the heterogeneous catalytic process played an important role in TOC removal.

The complete mineralization of OG could be described by Eq. (2) below,

$$C_{16}H_{10}N_2Na_2O_7S_2 + 42H_2O_2 \rightarrow 16CO_2 + 2HNO_3 + 2NaHSO_4 + 45H_2O \quad (2)$$

According to this equation, 157.8 mg L^{-1} of H_2O_2 is theoretically needed to completely mineralize 50 mg L^{-1} of OG, which is much higher than H_2O_2 addition used in this study. The following reasons may explain this phenomenon: (i) The adsorption of intermediate products on the surface of BT4,[48] (ii) The contribution of O_2 in photo-Fenton reactions.[49]

Fig. 4.

To quantify the adsorption of intermediate products on the surface of BT4, the solution pH was adjusted to 11 at the end of the reaction and the TOC removal efficiency dropped to about 60%, indicating approximate 18.9% of TOC was adsorbed on the surface of BT4.

The role of oxygen in the degradation of OG was investigated by bubbling nitrogen instead of air in the $UV/H_2O_2/BT4$ system. As shown in Fig. 5, both decolorization and TOC removal rates of OG decreased when air was replaced by nitrogen. The attack of organic species (RH) by $^{\bullet}OH$ generates the organic radical ($R^{\bullet}$) via Eq. (3). In the presence of O_2 (air), the organic radical would be converted to a peroxo-organic radical $ROO^{\bullet}$ as indicated in Eq. (4), which in turn could participate in the series of reactions through Eq. (5):[37,46, 50-52]

$$RH + {}^{\bullet}OH \rightarrow R^{\bullet} + H_2O \quad (3)$$

$$R^{\bullet} + O_2 \rightarrow ROO^{\bullet} \quad (4)$$

$$ROO^{\bullet} + H_2O \rightarrow \text{intermediates} + HO_2^{\bullet} \quad (5)$$

Therefore, after 180 min reaction, 78.9% of TOC removal efficiency was achieved by $UV/H_2O_2/BT4$ when oxygen was present, while only 38.4% TOC was removed in the presence of nitrogen and more organics (23.0% of TOC) would be desorbed from catalyst particles when the solution pH was adjusted to 11 at the end of the reaction.

Fig. 5.

The carboxylic acids, such as adipic acid (G), citric acid (H), and oxalic acid (I), were detected by IC during the degradation of OG. These carboxylic acids would complex with $\equiv Fe^{3+}$ to form $\equiv FeR(COO)_n^{(n-3)-}$. The ferric carboxylate complexes could be photolyzed to generate $\equiv Fe^{2+}$ and carboxylate radical ($R(COO)_n^{\bullet -}$) in acid solution via Eq. (6).[50,53] In air-saturated acid solution, the carboxylate radical reacts with molecular oxygen to form the hydroperoxyl radical ($O_2^{\bullet -}$) through Eq. (7), which disproportionates to produce H_2O_2.[50,54] The generated H_2O_2, as the additional oxidant, is decomposed to generate $^{\bullet}OH$, resulting in the improvement of the TOC removal. Therefore, the $UV/H_2O_2/BT4$ system could achieve higher decolorization efficiency than dark system, as illustrated in Fig. 3.

$$\equiv FeR(COO)_n^{(n-3)-} \xrightarrow{h\nu} \equiv Fe^{2+} + R(COO)_n^{\bullet -} + \text{intermediates} \quad (6)$$

$$R(COO)_n^{\bullet -} + O_2 \rightarrow \text{intermediates} + CO_2 + O_2^{\bullet -} \quad (7)$$

Based on the results and previous literatures, a possible mechanism of colour and TOC removal in the $UV/BT4/H_2O_2$ system was proposed and illustrated in Fig. 6. The $^{\bullet}OH$ was generated by activation of H_2O_2 with $\equiv Fe^{2+}$ in the surface of BT4 or dissolved Fe^{2+}. Then, OG was oxidized by $^{\bullet}OH$ to form organic radical $R^{\bullet}$. The reaction of $R^{\bullet}$ with O_2 yielded peroxo-organic radical $ROO^{\bullet}$, which was further degraded to carboxylate. The carboxylate ion would complex with $\equiv Fe^{3+}$ to form ferric carboxylate and then produce carboxylate radical and $\equiv Fe^{2+}$ under UV irradiation. In presence of O_2, carboxylate radical could be degraded to smaller molecule compounds.

Fig. 6.

3.4 Stability and reusability of BT4

The morphology and functional groups of used BT4 were obtained and compared with those of fresh BT4 through SEM images and FTIR spectra, respectively. As illustrated in Fig. 7(a), the rough surface and amorphous structure of used BT4 were observed, which was similar to fresh BT4. In the meanwhile, there was little difference of FTIR spectra between fresh and used BT4 as depicted in Fig. 7(b). The band between 3000 and 3500 cm^{-1} is generated by the stretching of free/bonded hydroxyl groups.[55] The peaks at about 781 cm^{-1} and 789 cm^{-1} are attributed to O–H bending bands in goethite (Fe–OH) and are respectively on behalf of the vibration in and out of the plane.[55] The band absorption at 506 cm^{-1} is assigned to Fe–O stretching vibrations.[55,56]

Fig. 7.

In order to further confirm the stability of the BT4 catalyst, the reuse experiments were performed. Under the same conditions, the experiments of the catalytic degradation of OG were repeated for four cycles and each experiment was lasted for 90 min. The reused catalyst was filtered and rinsed with deionized water after each repeated experiment, then dried around 100 °C. As shown in Fig. 7(c), 99.1%, 89.4%, 91.1% and 91.1% of the OG removal were obtained in four successive cycles, respectively. The decolorization efficiency of OG is about 10% higher in the first cycle than that in the last three successive cycles. It was due to less leaching iron ion in the last three successive cycles. However, the decolorization efficiencies of OG were nearly the same in the last three successive cycles, indicating BT4 was an excellent long-term stable catalyst for the $UV/H_2O_2/BT4$ system.

3.5 Effects of important parameters on the decolorization of OG

Experiments under various reaction conditions (pH, H_2O_2 and catalyst addition) were conducted and the results were shown in Fig. 8. It can be seen from Fig. 8(a), the decolorization rate increased appreciably with initial pH decreasing from 6 to 3, but further decrease of initial pH to 2 led to an unpronounced increase of decolorization rate. Despite of this, the decolorization efficiency of OG was almost the same after 90 min reaction. It indicated that the proposed heterogeneous photo-Fenton process is efficient for colour removal under the pH range investigated.

Fig. 8.

The effect of BT4 addition on the OG decolourization is presented in Fig. 8(b). It was found that the decolourization rate increased with the increase of BT4 addition from 4 to 6 g L^{-1}. The increase of BT4 addition corresponds to the higher total specific area, resulting in the faster decomposition of H_2O_2 to generate $^{\bullet}OH$ for the decolorization of OG. However, the overdosed catalyst brought about the turbidity of the suspension and consequently the decrease of UV light penetration when BT4 addition increased over 6 g L^{-1}. Therefore, the removal rate of OG increased insignificantly with BT4 addition increasing from 6 to 8 g L^{-1}.

View Article Online
DOI: 10.1039/C5RA04258K

Fig. 8(c) illustrated that the decolorization rate increased with an increase in H_2O_2 concentration of up to 25 mg L^{-1}. Afterwards, the removal rate of OG was not improved obviously. It could be noticed that H_2O_2 is a source of $^{\bullet}OH$ in the UV/H_2O_2/BT4 system and the increase of H_2O_2 concentration would lead to more $^{\bullet}OH$ produced.[21,57] However, when H_2O_2 was excess, the generated $^{\bullet}OH$ would be consumed via the following reaction,[21,57]

$$H_2O_2 + {}^{\bullet}OH \rightarrow HO_2{}^{\bullet} + H_2O \quad (8)$$

After 90 min reaction, the decolorization efficiencies were almost the same with H_2O_2 concentration ranging from 25 to 100 mg L^{-1}, indicating that the generated $^{\bullet}OH$ were sufficient enough to achieve the almost complete colour removal.

3.6 The degradation pathway of OG

The changes of the absorption bands reflect the evolution of the chromophores of OG and useful information could be provided by the analysis of the UV-vis spectra. The UV-vis spectral changes as the reaction time are shown in Fig. 9(a). As can be seen from Fig. 9(a), The UV-vis spectrum of the untreated initial solution of OG recorded at pH 3 shows three main absorption peaks at 480, 330, and 250 nm, as well as a shoulder peak at 400 nm. The peak at 480 nm was attributed to the absorption of the $\pi \rightarrow \pi^*$ transition related to the –N=N– group, while additional bands at 250 and 330 nm were assigned to the $\pi \rightarrow \pi^*$ transition of benzene and naphthalene rings in the OG molecule, respectively.[6,12,24] Moreover, the absorption peak at 480 nm decreased rapidly and essentially disappeared with the reaction proceeded after 90 min reaction, indicating that the azo bonds (–N=N–) and conjugated π^* systems were completely destroyed. In addition, the other two absorption peaks around 250 and 330 nm declined slowly, illustrating that the aromatic rings were still present.

GC/MS analysis was employed to further identify the intermediate products during the OG degradation process. The by-products, such as aniline (A), 2-aminophenol (B), 4-nitrophenol (C), phenol (D), benzoquinone (E), and 3-nitropropanoic acid (F), were detected. Based on the IC and GC/MS results as well as previous studies,[8,58-62] the plausible degradation pathway of OG by UV/H_2O_2/BT4 is proposed in Fig. 9(b).

Fig. 9.

As indicated in Fig. 9(b), the first step of oxidation is the cleavage of −N=N−, resulting in the production of aniline (A) and 7-hydroxy-8-(hydroxyamino) naphthalene-1,3-disulfonic acid.[58,62] The intermediate products underwent complicated degradation reactions in which naphthalene rings were broken and aniline (A) was further attacked by $^{\bullet}OH$, resulting in the formation of 2-aminophenol (B), 4-nitrophenol (C) and phenol (D). These products were then degraded into benzoquinone (E), and the carboxylic acids such as 3-nitropropanoic acid (F), adipic acid (G), citric acid (H) and oxalic acid (J) were formed with the destruction of the aromatic ring. Finally, these carboxylic acids were degraded into smaller molecule compounds.

4. Conclusion

In this study, the BT4 catalysts have been found to be efficient and environmental benign for the heterogeneous activation of H_2O_2 in the presence of UV irradiation. OG could be quickly decolorized under the conditions investigated and the decolorization efficiency was still over 89% after four cycles. 78.9% of TOC removal was obtained at 50 mg L^{-1} initial OG concentration, 25 mg L^{-1} H_2O_2 concentration, pH = 3 and 6 g L^{-1} BT4 addition. As clearly proved by UV-vis, IC and GC/MS analysis, OG quickly reacted with free radical, resulting in the cleavage of azo-bond, followed by a series of degradation reactions of OG. The coupled UV/H_2O_2/BT4 system appears as a promising process for the dye wastewater treatment.

Acknowledgements

This work was supported by Natural Science Foundation of Hubei Province, China (Grant 2012FFA089) and the National Science Council of the Republic of China (No.NSC102-2622-E-006-004-CC2).

Notes references

[a] Department of Environmental Engineering, Wuhan University, P.O. Box C319, Luoyu Road 129#, Wuhan 430079, China

b Department of Environmental science and Engineering, Anhui science and technology University, Donghua Road 9#, Fengyang 233100, China

c Department of Chemical Engineering, National Cheng Kung University, Tainan 701, Taiwan

d Sustainable Environmental Research Center, National Cheng-Kung University, Tainan 701, Taiwan

† Corresponding author. Tel.: +86 27 68775837; fax: +86 27 68778893; E-mail address: eeng@whu.edu.cn (H. Zhang).

Corresponding author. Tel:+ 886-2757575x62636; fax: + 886-6-2344496; E-mail address: yhhuang@mail.ncku.edu.tw (Y.H. Huang).

Reference

1 N. Panda, H. Sahoo and S. Mohapatra, *J. Hazard. Mater.,* 2011, **185**, 359–365.

2 Y.W. Gao, Y. Wang and H. Zhang, Appl. *Catal. B: Environ.,* 2014, http://dx.doi.org/10.1016/j.apcatb.2014.11.005.

3 M.L. Rache, A.R. García, H.R. Zea and A.M.T. Silva, *Appl. Catal. B: Environ*., 2014, **146**, 192– 200.

4 H.Y. Li, Y.L. Li, L.J. Xiang, Q.Q. Huang, J.J. Qiu, H. Zhang, M.V. Sivaiah, F. Baron, J. Barrault, S. Petit and S. Valange, *J. Hazard. Mater*., 2015, **287**, 32–41.

5 A. Ajmal, I. Majeed, R.N. Malik, H. Idriss and M.A. Nadeem, *RSC Adv*., 2014, **4**, 37003–37026.

6 C.G. Niu, Y. Wang, X.G. Zhang, G.M. Zeng, D.W. Huang, M. Ruan and X.W. Li, *Bioresour. Technol*., 2012, **126**, 101–106.

7 A. El-Ghenymy, F. Centellas, J.A. Garrido, R.M. Rodríguez, I. Sirés, P.L. Cabot and E. Brillas, *Electrochim. Acta*, 2014, **130**, 568–576.

8 M.Q. Cai, M.C. Jin and L.K. Weavers, Ultrason. Sonochem. 2011, 18, 1068–1076.

9 L. Doumic, G. Salierno, M. Cassanello, P. Haure and M. Ayude, *Catal. Today*, 2015, **240**, 67–72.

10 L. Zhang, Z.J. Cheng, X. Guo, X.H. Jiang and R. Liu, *J. Mol. Liq*. 2014, **197**, 353–367.

11 A. Tripathi and S.K. Srivastava, Afr. J. Biotechnol. 2012, **11**, 1768–1781.

12 V. Dulman, S.M. Cucu-Man, R.I. Olariu, R. Buhaceanu, M. Dumitraş and I. Bunia, *Dyes Pigments*, 2012, **95**, 79-88.

13 S.M. Ghoreishian, K. Badii, M. Norouzi, A. Rashidi, M. Montazer, M. Sadeghi and M. Vafaee, *J. Taiwan Inst. Chem. Eng.*, 2014, **45**, 2436–2446.

14 J. Wu, F. Liu, H. Zhang, J.H. Zhang and L. Li, Desalin. Water Treat., 2012, **44**, 36–43.

15 H. Lachheb, E. Puzenat, A. Houas, M. Ksibi, E. Elaloui, C. Guillard, J. Herrmann, Appl. Catal. B: Environ. 2002, **39**, 75–90.

View Article Online
DOI: 10.1039/C5RA04238K

ARTICLE

16 X. Florenza, A.M.S. Solano, F. Centellas, C.A. Martínez-Huitle, E. Brillas and S. Garcia-Segura, *Electrochim. Acta*, 2014, **142**, 276–288.

17 G. Kumaravel Dinesh, S. Anandan and T. Sivasankar, *RSC Adv.*, 2015, **5**, 10440–10451.

18 H. Zhang, Y. Zhang and D.B. Zhang, Color. Technol., 2007, **123**, 101–105.

19 H. Zhang, J.H. Zhang, C.Y. Zhang, F. Liu and D.B. Zhang, Ultrason. Sonochem., 2009, **16**, 325–330.

20 H. Kusic, I. Peternel, N. Koprivanac and A. Loncaric Bozic, J. Environ. Eng., 2011, **137**, 454–463.

21 H. Zhang, H. Fu and D.B. Zhang, J. Hazard. Mater., 2009, **172**, 654–660.

22 R. Liu, D.X. Xiao, Y.G. Guo, Z.H. Wang and J.S. Liu, *RSC Adv*., 2014, **4**, 12958–12963.

23 H. Zhang, H. Fu, Y. Wang and L. Chen, Environ. Eng. Manage. J., 2015, **14**, 737–744.

24 M.Q. Cai, X.Q. Wei, Z.J. Song and M.C. Jin, *Ultrason. Sonochem*., 2015, **22**, 167–173.

25 Y. H. Gong, H. Zhang, Y. L. Li, L. J. Xiang, S. Royer, S. Valange and J. Barrault. *Water Sci. Technol.,* 2010, **62**: 1320–1326.

26 F. Duarte and L.M. Madeira, *Sep. Sci. Technol*., 2010, **45**, 1512–1520.

27 X. Zhong, S. Royer, H. Zhang, Q.Q. Huang, L.J. Xiang, S. Valange and J. Barrault. *Sep. Purif. Technol.*, 2011, **80**: 163–171.

28 H.H. Wu, X.W. Dou, D.Y. Deng, Y.F. Guan, L.G. Zhang and G.P. He, *Environ. Technol*., 2012, **33**, 1545–1552.

29 H. Zhang, H. Gao, C. Cai, C.Y. Zhang and L. Chen, Water Sci. Technol., 2013, **68**, 2515–2520.

30 L.W. Hou, Q.H. Zhang, F. Jérôme, D. Duprez, H. Zhang and S. Royer, Appl. Catal. B: Environ., 2014, **144**, 739–749.

31 Y. Wang, Y.W. Gao, L. Chen and H. Zhang, Catal. Today, 2015, DOI: 10.1016/j.cattod.2015.01.012

32 C.C. Chang, Y.H. Huang and H.T. Chen, *Sep. Sci. Technol*., 2010, **45**, 370–379.

33 C.H. Liu, Y.J. Shih, Y.H. Huang and C.P. Huang, *J. Taiwan Inst. Chem. Eng.,* 2014, **45**, 914–920.

34 H.Y. Li, R. Priambodo, Y. Wang, H. Zhang and Y.H. Huang, *J. Taiwan Inst. Chem. Eng*., 2015, DOI: 10.1016/j.jtice.2015.02.024.

35 C.C. Su, C.M. Chen, J. Anotai and M.C. Lu, *Chem. Eng. J*., 2013, **222**, 128–135.

36 F. Tisa, A.A.A. Raman and W.M. A. W. Daud, J. Environ. Manage., 2014, **146**, 260–275.

37 Y.J. Shih, M.t. Tsai and Y.H. Huang, Water Res., 2013, **47**, 2325–2330.

38 W. Nam, K.Woo and G.Y. Han, *J. Ind. Eng. Chem*., 2009, **15**, 348–53.

39 H.C. Lan, A.M. Wang, R.P. Liu, H.J. Liu and J.H. Qua, *J. Hazard. Mater.*, 2015, **285**, 167–172.

40 J. Guo, Y.Y. Du, Y.Q Lan and J.D. Mao, *J. Hazard. Mater.*, 2011, **186**, 2083–2088.

41 K. Rusevova, F. Kopinke and A. Georgi, *J. Hazard. Mater.*, 2012, **241–242**, 433– 440.

42 Z.H. Xu, J.R. Liang and L.X. Zhou, *J. Alloys Compd.,* 2013, **546**, 112–118.

43 X.N. Fei , W.Q. Li , L.Y. Cao , J.H. Zhao and Y. Xia, *Desalin. Water Treat.,* 2013, **51**, 4750–4757.

44 Y. Liu and D.Z. Sun, *J. Hazard. Mater.*, 2007, **143**, 448–454.

45 S.R. Pouran, A.A.A. Raman and W.M.A.W. Daud, *J. Clean. Prod.*, 2014, **64**, 24–35.

46 F. Duan, Y.Z. Yang, Y.P. Li, H.B. Cao, Y. Wang and Y. Zhang, *J. Environ. Sci*., 2014, **26**, 1171–1179.

47 C.P. Huang and Y.H. Huang, App. Catal. A: General, 2009, **357**, 135–141.

48 C.L. Hsueh, Y.H. Huang , C.C. Wang and C.Y. Chen, Chemosphere, 2005, **58**, 1409–1414.

49 B. Utset, J. Garcia, J. Casado, X. Domènech and J. Peral, Chemosphere, 2000, **41**, 1187–1192.

50 Y.H. Huang, S.T. Tsai, Y.F. Huang and C.Y. Chen, *J. Hazard. Mater*., 2007, **140**, 382–388.

51 S.M. Kim and A. Vogelpohl, *Chem. Eng. Technol.*, 1998, **21**, 187–191.

52 Y.X. Du, M.H. Zhou and L.C. Lei, *Water Res.*, 2007, **41**, 1121–1133.

53 M.S. Lucas and J.A. Peres, *Dyes Pigments*, 2007, **74**, 622–629.

54 B.C. Faust and R.G. Zepp, *Environ. Sci. Technol.*, 1993, **27**, 2517–2522.

55 L.C.A. Oliveira, T.C. Ramalho, E.F. Souza, M. Gonçalves, D.Q.L. Oliveira, M.C. Pereira and J.D. Fabris, *Appl. Catal. B: Environ.*, 2008, **83**, 169–176.

56 N. Sankararamakrishnan, A. Gupta and S.R. Vidyarthi, *J. Environ. Chem. Eng.*, 2014, **2**, 802–810.

57 J. Herney-Ramirez, M.A. Vicente and L.M. Madeira, *Appl. Cataly. B: Environ.,* 2010, **98**, 10–26.

58 J. Madhavan, F. Grieser and M. Ashokkumar, *Ultrason. Sonochem*., 2010, **17**, 338–343.

59 X.R. Wang, P.X. Wu, Y.H. Lu, Z.J. Huang, N.W. Zhu and C. Lin, Z. Dang, *Sep. Purif. Technol.*, 2014, **132**, 195–205.

60 S. Rodriguez, L. Vasquez, D. Costa, A. Romero and A. Santos, *Chemosphere*, 2014, **101**, 86–92.

61 U. Riaz, S.M. Ashraf and A. Ruhela, *J. Environ. Chem. Eng.*, 2015, **3**, 20–29.

62 A.D. Bokare, R.C. Chikate, C.V. Rode and K.M. Paknikar, *Appl. Catal. B: Environ*., 2008, **79**, 270–278.

View Article Online
DOI: 10.1039/C5RA04238K

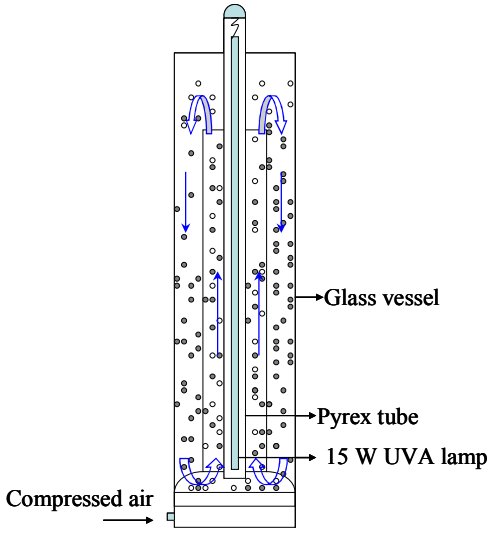

Fig. 1. The experimental set up

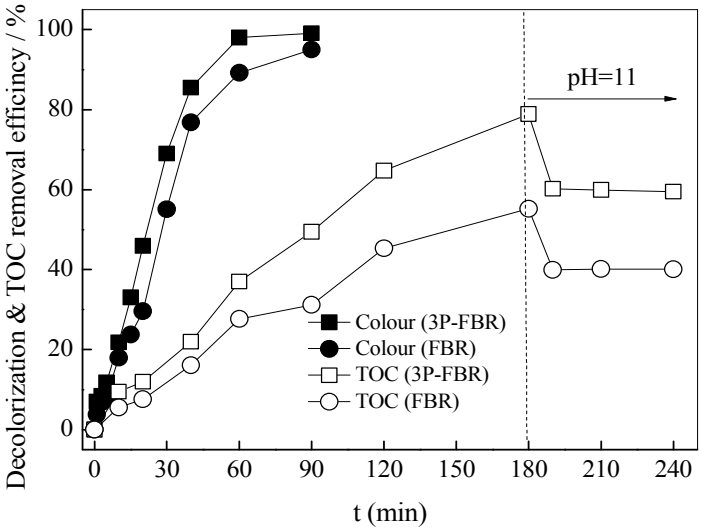

Fig. 2. Comparison of OG degradation in 3P-FBR and conventional FBR ([OG] = 50 mg L^{-1}, [H_2O_2] = 25 mg L^{-1}, pH = 3, [BT4] = 6 g L^{-1})

View Article Online
DOI: 10.1039/C5RA04238K

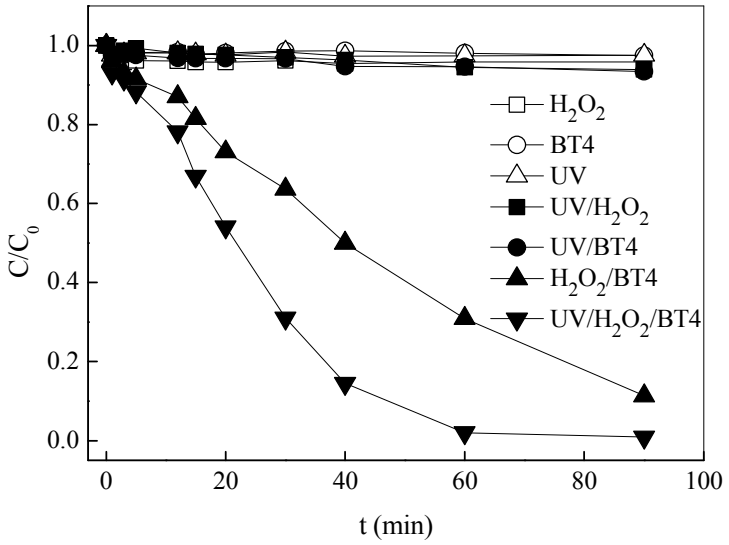

Fig. 3. Decolorization of OG by different processes ([OG] = 50 mg L^{-1}, [H_2O_2] = 25 mg L^{-1}, pH = 3, [BT4] = 6 g L^{-1})

(a)

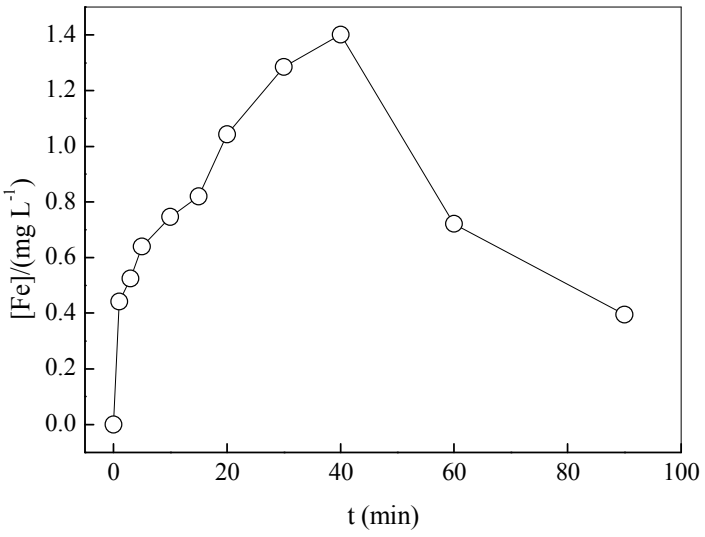

Fig. 4. (a) The changes of total dissolved iron concentration with reaction time, (b) the decolorization and the mineralization of OG in homogenous photo-Fenton process and heterogeneous photo-Fenton process ([OG] = 50 mg L^{-1}, [H_2O_2] = 25 mg L^{-1}, pH = 3, [BT4] = 6 g L^{-1}, [Fe^{2+}] = 1.4 mg L^{-1})

View Article Online
DOI: 10.1039/C5RA04238K

(b)

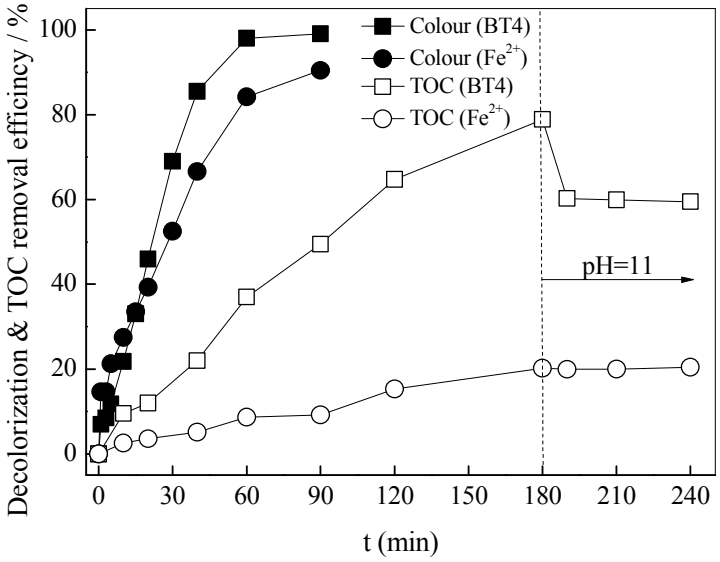

Fig. 4. Continue

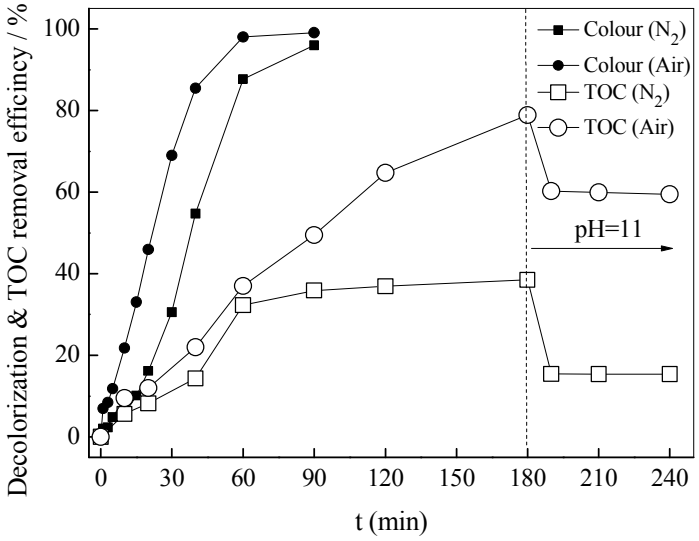

Fig. 5. Effect of dissolved gas on the decolorization and mineralization of OG ([OG] = 50 mg L^{-1}, [H_2O_2] = 25 mg L^{-1}, pH = 3, [BT4] = 6 g L^{-1})

View Article Online
DOI: 10.1039/C5RA04238K

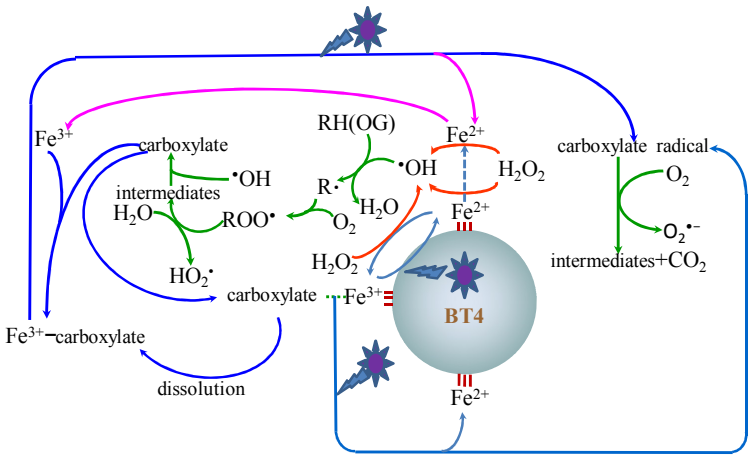

Fig. 6. Possible mechanism under UV/H_2O_2/BT4 system

(a)

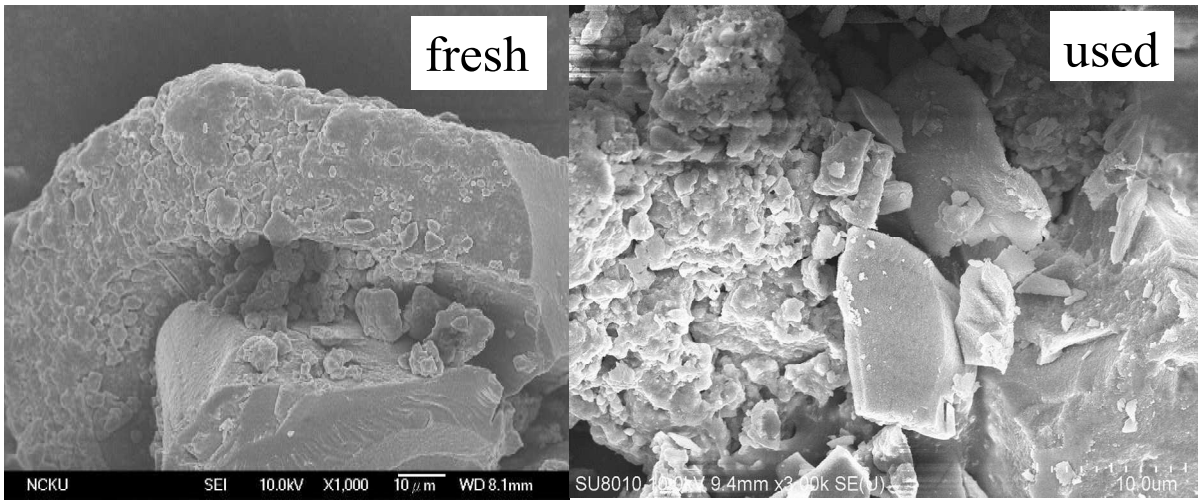

Fig. 7. (a) SEM image of fresh and used BT4, (b) FTIR spectra of fresh and used BT4 (c) the reusability of BT4 ([OG] = 50 mg L^{-1}, [H_2O_2] = 25 mg L^{-1}, pH = 3, [BT4] = 6 g L^{-1})

View Article Online
DOI: 10.1039/C5RA04238K

(b)

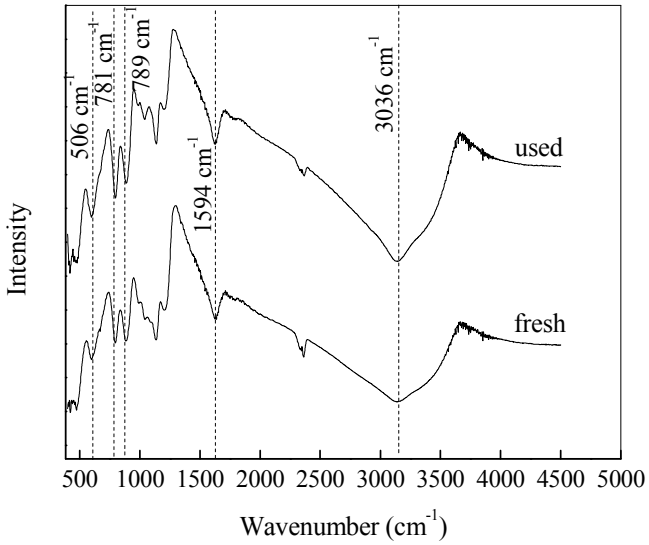

(c)

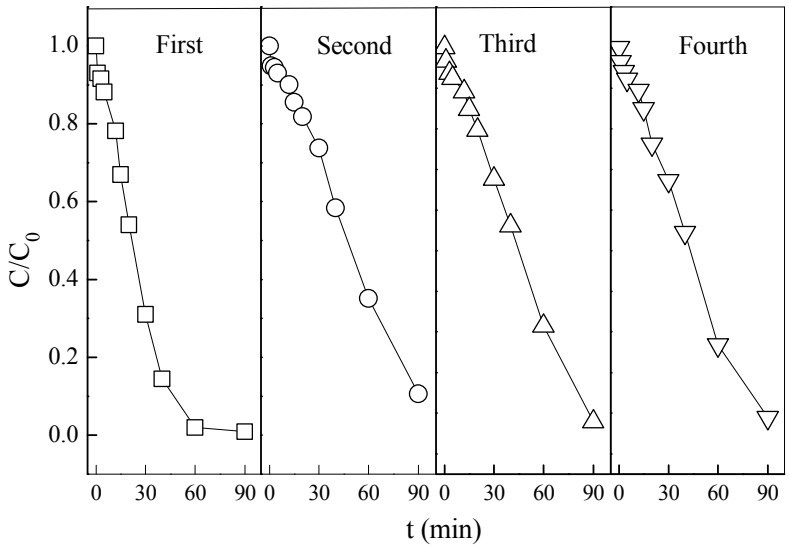

Fig. 7.Continue

View Article Online
DOI: 10.1039/C5RA04238K

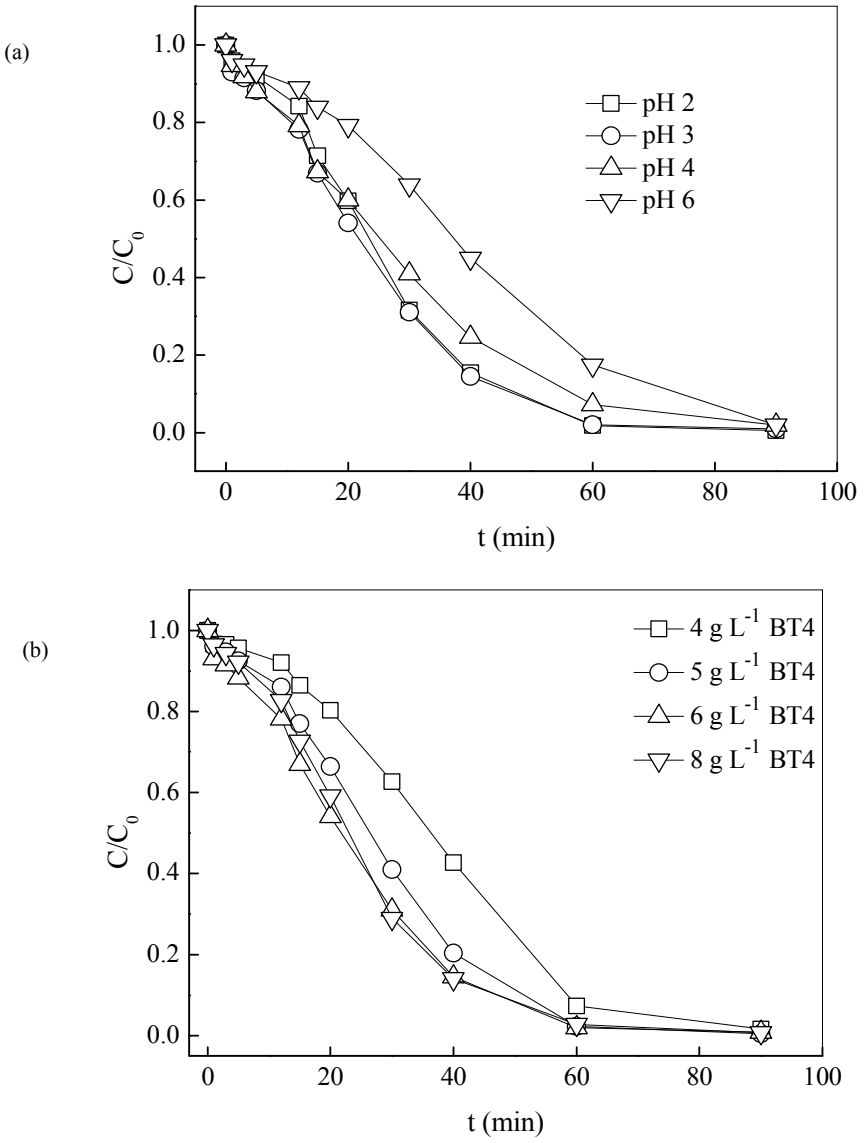

Fig. 8. Effect of major parameters on the OG removal: (a) pH, (b) BT4 addition, and (c) H_2O_2 concentration ([OG] = 50 mg L^{-1}, [H_2O_2] = 25 mg L^{-1}, pH = 3, [BT4] = 6 g L^{-1})

View Article Online
DOI: 10.1039/C5RA04238K

(c)

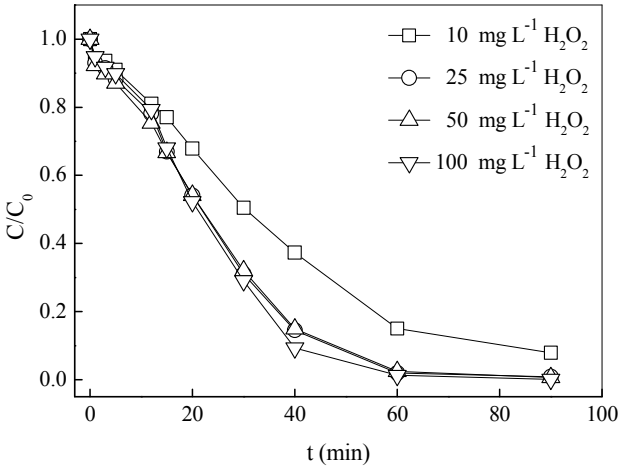

Fig. 8.Continue

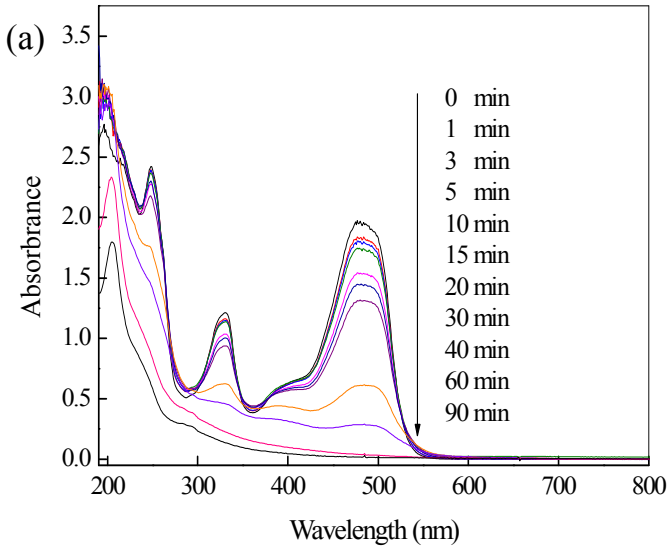

Fig. 9. (a) UV–vis spectral changes with reaction time and (b) proposed degradation pathway of OG ([OG] = 50 mg L^{-1}, [H_2O_2] = 25 mg L^{-1}, pH = 3, [BT4] = 6 g L^{-1})

View Article Online
DOI: 10.1039/C5RA04238K

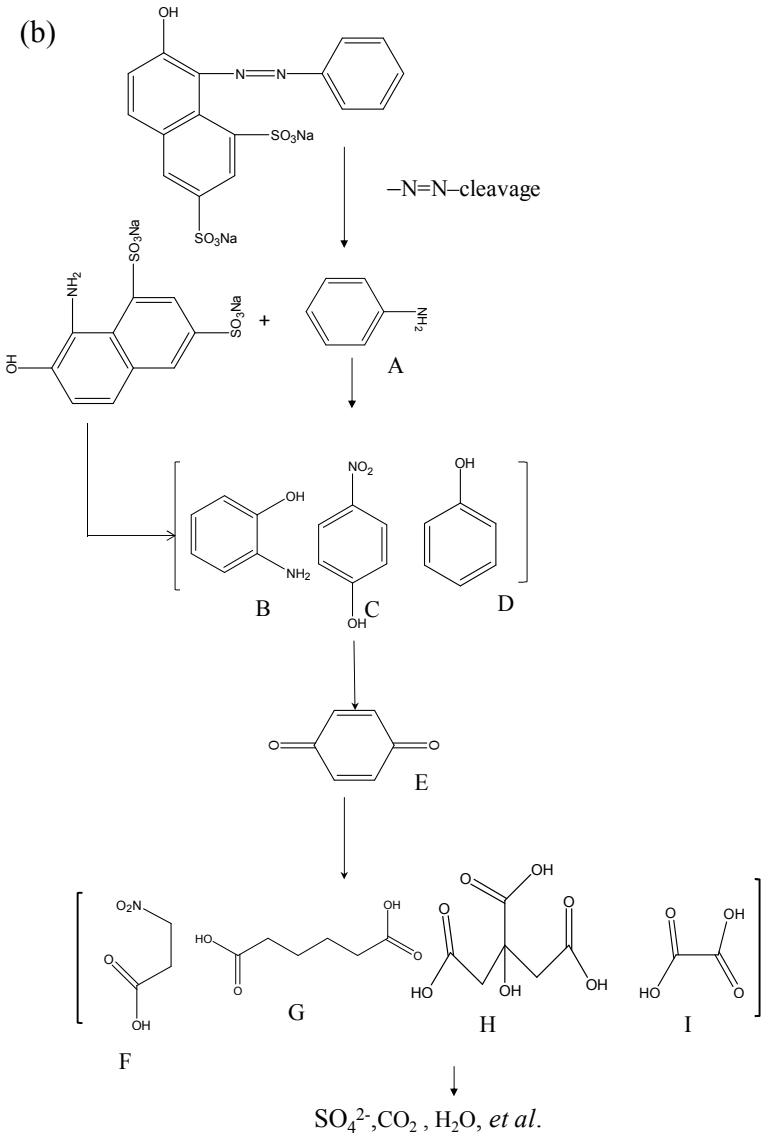

Fig. 9.Continue